IEEE Access
Multidisciplinary | Rapid Review | Open Access Journal

Received October 5, 2019, accepted October 22, 2019, date of publication October 25, 2019, date of current version November 6, 2019.

*Digital Object Identifier 10.1109/ACCESS.2019.2949642*

# All-Pass Negative Group Delay Function With Transmission Line Feedback Topology

**BLAISE RAVELO, (Member, IEEE), FAYU WAN, (Member, IEEE), AND JIAO FENG**
School of Electronic and Information Engineering, Nanjing University of Information Science and Technology (NUIST), Nanjing 210044, China

Corresponding author: Fayu Wan (fayu.wan@nuist.edu.cn)

This research work was supported in part by NSFC under Grant 61971230 and 61601233, and in part by Jiangsu Distinguished Professor program and Six Major Talents Summit of Jiangsu Province (2019-DZXX-022), and in part by the Postgraduate Research & Practice Innovation Program of Jiangsu Province under Grant SJKY19_0974, and in part by the Priority Academic Program Development of Jiangsu Higher Education Institutions (PAPD) Fund.

**ABSTRACT** A novel circuit theory of all-pass Negative group delay (NGD) function is investigated. The NGD function is implemented with unity direct chain feedback (UDCF) system. The active circuit is built with an operational amplifier in feedback with a lossy transmission line (TL). The UDCF topology S-parameter model is established versus TL parameters. The NGD analysis is elaborated from the frequency dependent transmission coefficient. The NGD behavior characterization is developed. The synthesis method allowing to determine the UDCF topology parameters in function of the targeted NGD values, gain and reflection coefficient is formulated. The all-pass NGD function is validated with a proof-of-concept (POC) design. Frequency and time domain simulations confirm the feasibility of the innovative all-pass NGD function. With S-parameter analysis, it was shown that the UDCF circuit exhibits NGD up to −7-ns with gain more than 0-dB and reflection coefficient −20-dB. More importantly, time-domain analysis illustrates how the transient tested voltage outputs can be in advance compared to the input.

**INDEX TERMS** All-pass NGD function, circuit theory, negative group delay (NGD), unit direct chain feedback (UDCF), S-parameter modeling, transmission line (TL).

## I. INTRODUCTION

Despite the spectacular development of the modern technology, the delay effect remains an open problem in several areas of engineering [1]–[4]. The performances of electrical, electronic, automatic and many more systems depend undesirably to the delay effects. The analytical link between the delay and system operation can be quantified from the system transfer functions. The system unit-step and harmonic responses illustrate how the delay degrade the performances. For example, the detrimental influence of time delays can be found in different aspects of automatic system analyses [5]–[7]. Among the concerning system, we can cite that very recently a prediction scheme for input delay was investigated [8], and a linear system stability condition was established as a function of the dwell-time parameters [9].

Nowadays, time delays constitute one of key parameters to be taken into account during the design and fabrication of automatic and electronic engineering systems. Improved studies on the time-delay effect are necessary during the engineering system design phase. Time-delay modules can be found at all levels of several engineering systems. For example, time-delay systems were applied to control the time lags used in vibrational feedback control [10]. An improved stabilization technique dedicated to linear systems with time delay has been proposed in [11]. Then, a delay-dependent H-infinity control of linear descriptor systems has been presented in [12]. It was underlined that delay-dependent criteria are required for robust stability analysis [13]. It has been reported in [14] that the time-delay systems stability problem involves an integral inequality. So far, the topic of innovative methods for time-delay systems is still very attractive for automatic and electronic design and simulation engineers.

The impact of signal propagation delay and group delays (GD) remains to be limiting factors for circuit operation speed [15]. Various tentative solutions of techniques using passive or active delay line system were developed. Nonetheless, considerable influences of signal delays are occurred in different frequency bands. The correction of

The associate editor coordinating the review of this manuscript and approving it for publication was Guangdeng Zong.


This work is licensed under a Creative Commons Attribution 4.0 License. For more information, see http://creativecommons.org/licenses/by/4.0/

these delays is still an open challenge for most of electronic design and research engineers. In addition to the noise effects, the GD impacts limit undesirably the radio frequency (RF) electronic device performances [16]. All-pass time-delay approximations for RF analog filters have been proposed in [17]. Generally, most of the proposed techniques to alleviate these undesirable effects are using positive time or GD which requires additional delay to the overall system.

However, an uncommon delay correction technique based on negative GD (NGD) less familiar to common electronic design and research engineers has been developed, too [18]. This counterintuitive technique is aimed to realize the signal delay cancellation. The basic principle consists in cascading positive and NGD circuits in order to generate a total GD equal to zero. Initially, the NGD circuits are implemented with low frequency operational amplifiers. The meaning of intriguing NGD phenomenon was demonstrated experimentally with the manifestation of signal time-advance [19]–[22]. The primitive theoretical and experimental studies were carried out with electronic circuits operating up to hundreds of kilohertz. It was emphasized that NGD phenomena do not contradict but are in fact required by causality [19], [20]. In addition, the existence of the NGD phenomenon has been demonstrated with the occurrence of signal advance [21], [22]. Otherwise, typically passive band-pass NGD circuits were also designed especially in RF and microwave frequencies. To do this, the NGD passive circuit was incorporated with a resonant filter function analytically related to the absorption effect [23]. Furthermore, the NGD effect was observed with audio signals in low frequency circuits [24] and within a photonic crystal structure [25].

By exploiting the NGD function, outstanding applications in various fields were developed. Several particular examples can be cited. In medical engineering, a system for real-time signal prediction has been proposed [26], [27]. It was hypothesized to be relevant in neural computation in general [28]. Furthermore, in automatic and control engineering, the NGD prediction could be used to realize high-performance robots which can be integrated particularly in the human motor control system [29]. It stands to reason that the utilization of NGD in applications has implicit limits. For example, in the one hand, certain feedback type NGD topologies could not be used in the wideband frequencies due to instabilities and long transients in linear systems [30], [31]. In the other hand, the NGD function generation in passive circuits is accompanied by signal absorption inducing inherent losses [32], [33]. To overcome the latter effect, active circuit topologies based on the use of RF transistors have been developed recently [34]. Moreover, it has been found that the NGD behaviors are similar to the linear filter gain [36], [37]. This similarity affirms the possibility of NGD function implementations in electrical and other systems.

In the present paper, a novel NGD topology is developed by exploiting the feedback delay concept. In difference to the research work published in [38]–[40], this unity direct chain feedback (UDCF) system study is completely original on the following points:

- The proposed circuit theory explains innovatively the design of typically all-pass NGD function,
- The all-pass NGD topology investigated is built with an operational amplifier in feedback lossy transmission line (TL),
- The new circuit theory is established with S-parameter modelling,
- And most importantly the NGD analysis and existence expressions are completely new.

The paper is mainly organized in five principal sections as follows. Section II is focused on the S-parameter modelling of the UDCF topology. The modelling is realized from the feedback chain matrix which is mainly calculated from the TL ABCD matrix. Section III elaborates the analytical expressions of the transmission coefficient magnitude, phase and GD. The UDCF NGD analysis and characterization are developed in Section IV. Very original expressions of NGD at different particular frequencies depending on the feedback line delay are established. Mathematical conditions illustrating the all-pass NGD function are discussed. Section V is essentially focused to the innovative all-pass NGD function validation by using a commercial electronic circuit simulation tool. Parametric analyses based on numerical modelling will be compared with theoretical calculations. This parametric analysis includes the influence of realistic operational amplifier parameter. As proof-of-concept (POC), comparisons between the calculated and simulated results in both the frequency and time domain are introduced and discussed. The paper is ended with a conclusion in Section VI.

## II. THEORETICAL INVESTIGATION ON THE DELAY TL FEEDBACK BASED UNITY DIRECT CHAIN FEEDBACK (UDCF) TOPOLOGY

The present section will begin with the identification of the UDCF circuit topology. The equivalent S-parameter will be modelled. The most important novel part of the paper concerning the NGD analysis will be developed. Then, the synthesis method of the UDCF topology will be formulated.

### A. UDCF TOPOLOGY NGD ANALYSIS

An implementation of positive delay network constitutes intuitively, the simplest solution to implement the feedback network. The NGD topological identification primes to the UDCF cell depicted in Fig. 1. In this topology, the resistance $R$ is inserted in the circuit in order to ensure the UDCF stability. The feedback network consists of a lossy TL, which will be defined analytically in the next paragraph, associated to the shunt resistance $R_x$.

#### 1) RECALL ON THE TL ABCD MATRIX

By denoting $\omega$ the angular frequency variable, the feedback lossy TL of the topology introduced in Fig. 1 is defined by:

- the characteristic impedance $Z(j\omega)$,
- the delay $\tau_0(\omega)$,

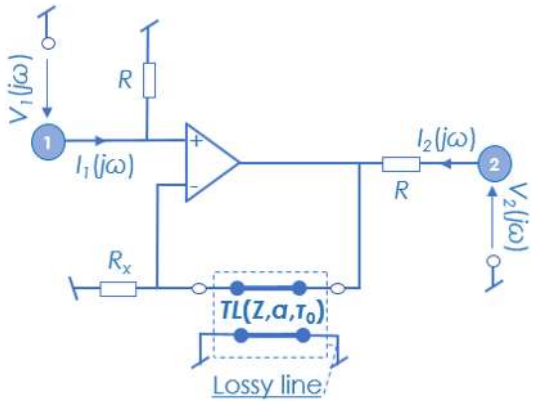


**FIGURE 1.** UDCF topology constituted by an amplifier operational in feedback with delay lossy TL.

- and the attenuation loss $a(\omega)$.

Under this configuration, the TL phase can be expressed as:

$$\varphi_{TL}(\omega) = -\int \tau_0(\omega) d\omega. \tag{1}$$

Based on the TL theory, the ABCD matrix is analytically defined by:

$$[T(j\omega)] = \begin{bmatrix} T_1(\omega) & Z(j\omega)T_2(\omega) \\ \dfrac{T_2(\omega)}{Z(j\omega)} & T_1(\omega) \end{bmatrix}, \tag{2}$$

with:

$$T_1(\omega) = \frac{e^{j\omega\tau_0(\omega)} + a^2(\omega)e^{-j\omega\tau_0(\omega)}}{2a(\omega)}, \tag{3}$$

$$T_2(\omega) = \frac{e^{j\omega\tau_0(\omega)} - a^2(\omega)e^{-j\omega\tau_0(\omega)}}{2a(\omega)}. \tag{4}$$

#### 2) RECALL ON THE OPERATIONAL AMPLIFIER BASED FEEDBACK CIRCUIT CHARACTERISTIC

As mentioned in Fig. 1, the UDCF topology analysis depends on the electrical parameters of access ports ❶ and ❷. With the black box approach, the main parameters are:

- The general input and output voltages $V_1(j\omega)$ and $V_2(j\omega)$, respectively,
- And the general input and output currents propagating through the access ports $I_1(j\omega)$ and $I_2(j\omega)$, respectively.

In this paper, to simplify the analytical expression, the operational amplifier is assigned with voltage conversion gain as an independent frequency real positive quantity:

$$G(j\omega) \approx g. \tag{5}$$

### B. ANALYTICAL CHARACTERIZATION OF THE FEEDBACK CHAIN

According to the circuit and system theory, the ABCD equivalent matrix of the feedback TL and the shunt resistance $R_x$ is defined by the product:

$$[ABCD(j\omega)] = [T(j\omega)] \times \begin{bmatrix} 1 & 0 \\ \dfrac{1}{R_x} & 1 \end{bmatrix}. \tag{6}$$

Substituting $[T(j\omega)]$ with its expression introduced in (2), we obtain the following expression of the feedback chain matrix:

$$[ABCD(j\omega)] = \begin{bmatrix} T_1(\omega) + \dfrac{Z(j\omega)T_2(\omega)}{R_x} & Z(j\omega)T_2(\omega) \\ \dfrac{Z(j\omega)T_1(\omega) + R_xT_2(\omega)}{R_xZ(j\omega)} & T_1(\omega) \end{bmatrix}. \tag{7}$$

Acting as two-port system, the impedance- or Z-matrix is defined by:

$$\begin{bmatrix} V_1(j\omega) \\ V_2(j\omega) \end{bmatrix} = \begin{bmatrix} Z_{11}(j\omega) & Z_{12}(j\omega) \\ Z_{21}(j\omega) & Z_{22}(j\omega) \end{bmatrix} \begin{bmatrix} I_1(j\omega) \\ I_2(j\omega) \end{bmatrix}. \tag{8}$$

This ABCD matrix can be calculated from the basic principles of circuit theory. By taking into account the operational amplifier gain given in (1), we have:

$$[Z(j\omega)] = \begin{bmatrix} R & 0 \\ \dfrac{g \cdot R \cdot [R_xT_1(\omega) + Z(j\omega)T_2(\omega)]}{(1+g)R_xT_1(\omega) + Z(j\omega)T_2(\omega)} & R \end{bmatrix}. \tag{9}$$

It is noteworthy that only the element $Z_{21}(j\omega)$ depends on the TL chain matrix elements $T_1$ and $T_2$.

### C. S-PARAMETER MODELLING

Similar to all the classical microwave circuit, the S-parameter analysis of the UDCF topology introduced in this paper is performed assuming the reference impedance $R_0 = 50\ \Omega$. After the Z-to-S matrix transform, the S-parameters are extracted from the Z-matrix defined in (3) via the relationship [40]:

$$[S(j\omega)] = \left\{ \begin{array}{l} \left( [Z(j\omega)] - \begin{bmatrix} R_0 & 0 \\ 0 & R_0 \end{bmatrix} \right) \times \\ \left( [Z(j\omega)] + \begin{bmatrix} R_0 & 0 \\ 0 & R_0 \end{bmatrix} \right)^{-1} \end{array} \right\}. \tag{10}$$

This calculation implies the following expression of the UDCF topology S-parameters:

$$[S(j\omega)] = \begin{bmatrix} S_{11}(j\omega) & S_{12}(j\omega) \\ S_{21}(j\omega) & S_{22}(j\omega) \end{bmatrix}, \tag{11}$$

with:

- the isolation coefficient (the UDCF topology behaves as a unilateral circuit):

$$S_{12}(j\omega) = 0, \tag{12}$$

- the input and output reflection coefficients:

$$S_{11}(j\omega) = S_{22}(j\omega) = \frac{R - R_0}{R + R_0}, \tag{13}$$

- and the transmission coefficient:

$$S_{21}(j\omega) = \frac{2R_0R}{(R+R_0)^2} \frac{g\,[R_xT_1(\omega) + Z(j\omega)T_2(\omega)]}{(1+g)R_xT_1(\omega) + Z(j\omega)T_2(\omega)}. \tag{14}$$

## III. UDCF TRANSMITTANCE ANALYSIS

The frequency-dependent theoretical expressions of transmission coefficient magnitude and transmission phase are introduced in this section. Then, the calculation approach of the UDCF topology GD will be elaborated.

### A. TRANSMISSION GAIN AND PHASE OF THE PROPOSED UDCF TOPOLOGY

For the sake of the analytical simplification, we suppose that in the rest of the paper, the TL characteristic impedance, loss, and delay, respectively:

$$\begin{cases} Z(j\omega) = Z \\ a(\omega) = a \\ \tau_0(\omega) = \tau_0, \end{cases} \tag{15}$$

are constant or frequency independent factors. The detailed formulation of transmission coefficient derived from (14) can be written as:

$$T(j\omega) = \frac{2R_0Rg}{(R_0+R)^2} \frac{\left[a^2(R_x-Z)+(R_x+Z)e^{2j\omega\tau_0}\right]}{\left[\begin{matrix} a^2(R_x-Z)+2agR_xe^{j\omega\tau_0} \\ +(R_x+Z)e^{2j\omega\tau_0} \end{matrix}\right]}. \tag{16}$$

The corresponding magnitude $T(\omega) = |T(j\omega)|$ is equal to:

$$T(\omega) = \frac{\frac{2R_0Rg}{(R_0+R)^2}\sqrt{\left[\begin{matrix} a^2(R_x-Z)+ \\ (R_x+Z)\cos(2\omega\tau_0) \end{matrix}\right]^2 + (R_x+Z)^2\sin^2(2\omega\tau_0)}}{\sqrt{\left[\begin{matrix} a^2(R_x-Z)+2agR_x\cos(\omega\tau_0) \\ +(R_x+Z)\cos(2\omega\tau_0) \end{matrix}\right]^2 + \left[\begin{matrix} 2agR_x\sin(\omega\tau_0)+ \\ (R_x+Z)\sin(2\omega\tau_0) \end{matrix}\right]^2}}. \tag{17}$$

We remind that the corresponding transmission phase is mathematically given by:

$$\varphi(\omega) = \angle T(j\omega) = \arctan\left[\frac{Im\left[T(j\omega)\right]}{Re\left[T(j\omega)\right]}\right]. \tag{18}$$

This phase can be written as:

$$\varphi(\omega) = \varphi_a(\omega) + \varphi_b(\omega), \tag{19}$$

where:

$$\varphi_a(\omega) = \arctan\left[\frac{(R_x+Z)\sin(2\omega\tau_0)}{a^2(R_x-Z)+(R_x+Z)\cos(2\omega\tau_0)}\right], \tag{20}$$

$$\varphi_b(\omega) = -\arctan\left[\frac{\begin{matrix} 2agR_x\sin(\omega\tau_0)+ \\ (R_x+Z)\sin(2\omega\tau_0) \end{matrix}}{\begin{matrix} a^2(R_x-Z)+2agR_x\cos(\omega\tau_0) \\ +(R_x+Z)\cos(2\omega\tau_0) \end{matrix}}\right]. \tag{21}$$

### B. GD FORMULATION

We remind that the associated GD is mathematically defined by:

$$\tau(\omega) = -\frac{\partial\varphi(\omega)}{\partial\omega}. \tag{22}$$

By using (19), this GD can be expressed as:

$$\tau(\omega) = \tau_a(\omega) + \tau_b(\omega), \tag{23}$$

where:

$$\begin{cases} \tau_a(\omega) = -\dfrac{\partial\varphi_a(\omega)}{\partial\omega} \\ \tau_b(\omega) = -\dfrac{\partial\varphi_b(\omega)}{\partial\omega}. \end{cases} \tag{24}$$

After analytical calculation, we have:

$$\tau_a(\omega) = \frac{-2\tau_0\left[1+a^2\frac{R_x-Z}{R_x+Z}\cos(2\omega\tau_0)\right]}{a^4+\frac{(R_x-Z)^2+2a^2(R_x^2+Z^2)\cos(2\omega\tau_0)}{(R_x+Z)^2}}, \tag{25}$$

$$\tau_b(\omega) = \frac{-2\left\{\begin{matrix} 2agR_x\left\{\begin{matrix} agR_x\cos^2(\omega\tau_0) \\ +\cos(\omega\tau_0) \\ \left[\begin{matrix} 3(R_x+Z)\cos(2\omega\tau_0) \\ +a^2(R_x-Z) \end{matrix}\right] \end{matrix}\right\} \\ +\psi_n(\omega) \end{matrix}\right\}}{\begin{matrix} 4agR_x\left\{\begin{matrix} agR_x\cos^2(\omega\tau_0)+\cos(\omega\tau_0) \\ \left[\begin{matrix} (R_x+Z)\cos(2\omega\tau_0) \\ +a^2(R_x-Z) \end{matrix}\right] \end{matrix}\right\} \\ +\psi_d(\omega) \end{matrix}}\tau_0, \tag{26}$$

with:

$$\psi_n(\omega) = \begin{Bmatrix} (R_x+Z)^2\cos^2(2\omega\tau_0)+ \\ a^2(R_x^2-Z^2)\cos(2\omega\tau_0)+ \\ [(R_x+Z)\sin(2\omega\tau_0)+agR_x\sin(\omega\tau_0)] \\ [(R_x+Z)\sin(2\omega\tau_0)+2agR_x\sin(\omega\tau_0)] \end{Bmatrix}, \tag{27}$$

$$\psi_d(\omega) = \left\{\begin{matrix} (R_x+Z)^2\cos^2(2\omega\tau_0)+ \\ 2a^2(R_x^2-Z^2)\cos(2\omega\tau_0) \\ +\left[\begin{matrix} (R_x+Z)^2\sin^2(2\omega\tau_0)+ \\ 4agR_x(R_x+Z)\sin(\omega\tau_0)\sin(2\omega\tau_0) \\ +a^2(4R_x^2g^2\sin^2(\omega\tau_0)+a^2(R_x-Z)^2) \end{matrix}\right] \end{matrix}\right\}. \tag{28}$$

It is noteworthy that the transmission gain and the GD expressed in (17) and (23), respectively, behave as periodical functions.

### C. STABILITY ANALYSIS

Similar to the RC-circuit based UDCF topology investigated in [40], the present stability analysis is performed in two complementary ways. In the one side, it can be realized with the analysis of the transfer function represented by $S_{21}$. In the other side, it can be analyzed following the usual method employed in RF and microwave engineering. Hence, acting as two-port system, the stability can be also analyzed from the S-matrix via the Rollett stability factor.

According to the circuit and system theory, a system is unstable when the transfer function denominator is equal to zero. With the unknown $\omega$, it implies the following equation system from (16):

$$\begin{cases} \mathrm{Re}\left[denom\left[T(j\omega)\right]\right] = 0 \\ \mathrm{Im}\left[denom\left[T(j\omega)\right]\right] = 0, \end{cases} \tag{29}$$

$$\Rightarrow \begin{cases} \begin{bmatrix} a^2(R_x - Z) + 2agR_x \cos(\omega\tau_0) \\ +(R_x + Z)\cos(2\omega\tau_0) \end{bmatrix} = 0 \\ 2agR_x \sin(\omega\tau_0) + (R_x + Z)\sin(2\omega\tau_0) = 0. \end{cases} \quad (30)$$

The simplified equations can be written as:

$$\begin{cases} \cos^2(\omega\tau_0) + \dfrac{agR_x}{R_x + Z}\cos(\omega\tau_0) + \dfrac{a^2(R_x - Z)}{2(R_x + Z)} - 1 = 0 \\ \cos(\omega\tau_0) + \dfrac{agR_x}{R_x + Z} = 0. \end{cases} \quad (31)$$

However, intuitively, this equation system does not have any solution. Meanwhile that the expression of the transmission coefficient guarantees that the UDCF topology is conditionally stable. Moreover, the stability factor derived from the S-parameter can be defined as:

$$\mu(\omega) = \frac{1 - |S_{11}(j\omega)|^2}{|S_{12}(j\omega)S_{21}(j\omega)| + \left| \begin{matrix} S_{22}(j\omega) - S_{11}^*(j\omega) \\ \begin{bmatrix} S_{11}(j\omega)S_{22}(j\omega) \\ -S_{12}(j\omega)S_{21}(j\omega) \end{bmatrix} \end{matrix} \right|^2}, \quad (32)$$

with:

$$S_{11}^*(j\omega) = conj\left[S_{11}(j\omega)\right]. \quad (33)$$

By taking into account the S-parameters introduced in (11), this stability factor is transformed as:

$$\mu(\omega) = \frac{1}{|S_{11}(j\omega)|}, \quad (34)$$

which becomes:

$$\mu(\omega) = \frac{R + R_0}{|R - R_0|}. \quad (35)$$

We point out that this quantity is obviously higher than the unity:

$$\mu(\omega) > 1. \quad (36)$$

In conclusion, it means that the circuit proposed in Fig. 1 is unconditionally stable.

## IV. NGD ANALYSIS APPLIED TO THE TL BASED UDCF TOPOLOGY

The NGD analysis must start from the GD calculation from the transmission coefficient. Then, GD expressions at some particular frequencies depending on the feedback TL delay. The analysis consists in determining the UDCF parameters fulfilling the NGD existence condition:

$$\tau(\omega) < 0. \quad (37)$$

### A. IDENTIFICATION OF NGD CENTER FREQUENCIES

The NGD analysis can be methodologically started with the verification of low-pass NGD aspect from the expression of $\tau(\omega \approx 0)$. To verify the feasibility of the low-pass NGD function, the transmission coefficient magnitude:

$$T(\omega) = |T(j\omega)|, \quad (38)$$

and GD must be calculated analytically at very low frequency $\omega \approx 0$.

For the present study, our goal is originally to discover the possibility to generate a typically all-pass NGD function. To reach this aim, it could be judicious to determine the GDs at some frequencies. To do this, the reference fundamental angular frequency can be defined as:

$$\omega_0 = \frac{2\pi}{\tau_0}. \quad (39)$$

The associated harmonics multiple of this angular frequency expressed in function of the integer $m = \{0, 1, 2, \ldots\}$ are given by:

$$\omega(m) = \frac{m\omega_0}{4}. \quad (40)$$

In the one period, the family of these frequencies can be written as:

$$\omega(m) = \frac{(4m + 1)\omega_0}{4}, \quad (41)$$

$$\omega(m) = \frac{(2m + 1)\omega_0}{2}. \quad (42)$$

### B. GAIN AND GD AT THE NGD CENTER FREQUENCIES

Tables 1 and 2 summarize the particular values of the transmission coefficients and the GDs respectively. As illustrated in Table 1, the UDCF topology is a promising topology to operate with amplification at the different frequencies indicated in (40), (41) and (42). Table 2 addresses the calculated expressions of the GDs at the different frequencies indicated in (40), (41) and (42). It can be remarked that the GDs are independent to the resistor $R$. The mathematical exploration of these equations enables to perform the henceforth NGD analysis of the UCDF topology. We recall that the lossy feedback TL implies $a < 1$. The NGD existence condition (37), depends on the numerators and denominators of rational quantities (46), (47) and (48).

**TABLE 1.** Transmission coefficients at $\omega(m) = m\omega_0/4$ with $m$ integer.

| $\omega(m)$ | $\left\|S_{21}[\omega(m)]\right\|$ | |
|---|---|---|
| $m\omega_0$ | $\left\|S_{21}\right\| = \left\| \dfrac{\frac{2R_0Rg}{(R_0+R)^2}\left[a^2(R_x - Z) + R_x + Z\right]}{a^2(R_x - Z) + 2agR_x + R_x + Z} \right\|$ | (43) |
| $(1/4 + m)\omega_0$ | $\left\|S_{21}\right\| = \dfrac{\frac{2R_0Rg}{(R_0+R)^2}\left\|a^2(Z - R_x) + R_x + Z\right\|}{\sqrt{\left[R_x + Z + a^2(Z - R_x)\right]^2 + 4(agR_x)^2}}$ | (44) |
| $(1/2 + m)\omega_0$ | $\left\|S_{21}\right\| = \left\| \dfrac{\frac{2R_0Rg}{(R_0+R)^2}\left[a^2(R_x - Z) + R_x + Z\right]}{a^2(R_x - Z) - 2agR_x + R_x + Z} \right\|$ | (45) |

**TABLE 2.** GDs at $\omega(m) = m\omega_0/4$ with $m$ integer.

| $\omega(m)$ | $\tau[\omega(m)]$ | |
|---|---|---|
| $m\omega_0$ | $\tau = \dfrac{2agR_x \dfrac{(a^2-1)R_x-(1+a^2)Z}{(1+a^2)R_x+(1-a^2)Z}}{2agR_x+(1+a^2)R_x+(1-a^2)Z}\tau_0$ | (46) |
| $(1/4+m)\omega_0$ | $\tau = \dfrac{4(agR_x)^2 \dfrac{(R_x+Z)^2-a^4(R_x-Z)^2}{\left[(a^2-1)R_x-(1+a^2)Z\right]^2}}{4(agR_x)^2+a^4(R_x-Z)^2+(R_x+Z)^2+2a^2(Z^2-R_x^2)}\tau_0$ | (47) |
| $(1/2+m)\omega_0$ | $\tau = \dfrac{2agR_x \dfrac{(1-a^2)R_x+(1+a^2)Z}{(1+a^2)R_x+(1-a^2)Z}}{(1+a^2)R_x+(1-a^2)Z-2agR_x}\tau_0$ | (48) |

### C. MATHEMATICAL ANALYSIS ON THE NGD EXISTENCE CONDITION

The GDs expressed in Table 2 serve to verify explicitly the possibility to realize:

$$\tau\,[\omega(m)] < 0, \tag{49}$$

with the proposed UDCF topology. Accordingly, we have the following analytical inequations depending on the TL and resistive parameters

- For equations (46) and (47), it can be emphasized that the denominators are always positive:

$$\begin{cases} (1+a^2)R_x+(1-a^2)Z > 0 \\ 2agR_x+(1+a^2)R_x+(1-a^2)Z > 0. \end{cases} \tag{50}$$

  To get the NGD effect, the following condition must be fulfilled for equation (48):

$$(a^2-1)R_x-(1+a^2)Z < 0, \tag{51}$$

  This inequality is equivalent to:

$$\frac{Z}{R_x} > \frac{a^2-1}{a^2+1}. \tag{52}$$

  Or, this last condition is unconditionally satisfied for any parameters of the UDCF topology.
- The numerator of equation (46) is always positive:

$$\frac{(1-a^2)R_x+(1+a^2)Z}{(1+a^2)R_x+(1-a^2)Z} > 0. \tag{53}$$

- To get the NGD effect with the, the following condition must be fulfilled for equation (48):

$$(1+a^2)R_x+(1-a^2)Z-2agR_x > 0, \tag{54}$$

  which can be written as:

$$g > \frac{(1+a^2)R_x+(1-a^2)Z}{2aR_x}. \tag{55}$$

Consequently, the NGD existence conditions established from equations (46), (47) and (48) can be satisfied with certain values of parameters. It means that the UDCF cell behave simultaneously as low-pass and bandpass NGD functions. Knowing the periodicity of the GD expressed earlier in (23), the UDCF topology operate as a multiband NGD circuit.

### D. SYNTHESIS METHOD OF THE NGD UDCF CELL

The proposed synthesis approach is focused to the typical case of low-pass NGD circuit. It means that the mathematical synthesis equations are calculated from the UDCF response at very low frequencies. The synthesis equations established in this subsection are derived from the transmission gain in (43) and the GD in (44).

The NGD synthesis consists in determining the UDCF circuit operating with the desired specifications with real variables as:

- transmission gain $g_0 > 0$,
- reflection coefficient $r < -10$ dB,
- NGD level $\tau(0) = \tau_a < 0$,
- and NGD cut-off frequency.

In other words, it aims to calculate the UDCF circuit parameters $R$, $R_x$, $\tau_0$ and $a$. In certain cases, the synthesis can also integrate the choice of the operational amplifier via the parameter $g$. The unknown UDCF topology parameters are the roots of the following equations:

- input and output access matching:

$$S_{11}(\omega \approx 0) = S_{22}(\omega \approx 0) = r, \tag{56}$$

- transmission gain:

$$S_{21}(\omega \approx 0) = g_0, \tag{57}$$

- and NGD level:

$$\tau(0) = \tau_a. \tag{58}$$

#### 1) SYNTHESIS OF RESISTANCE R

The resistor $R$ can be calculated from equation (59). The synthesis formula is given by:

$$R = R_0\frac{1+r}{1-r}. \tag{59}$$

#### 2) SYNTHESIS FORMULATION OF THE OPERATIONAL AMPLIFIER GAIN

The operational amplifier parameter $g$ can be chosen by inverting equation (47). Accordingly, we have the following expression:

$$g = \frac{2g_0\left[(1+a^2)R_x+(1-a^2)Z\right]}{(1-a^2)(1-r^2)Z+\left[(1+a^2)(1-r^2)-4ag_0\right]R_x}. \tag{60}$$

In this case, a realistic positive value in function of the values of $a$ and $r$, is established from this last equation under the following condition:

$$g_0 < g_{0\,\max} = \frac{(1+a^2)(1-r^2)}{4a}. \tag{61}$$

#### 3) SYNTHESIS FORMULA OF $R_X$

This resistor parameter can be determined by inverting equation (43). It yields the following synthesis formula respectively:

$$R_x = Z\frac{(1-a^2)\left[g(1-r^2)-2g_0\right]}{2g_0(1+a^2)+g\left[4ag_0-(1-r^2)(1+a^2)\right]}. \quad (62)$$

To generate a realistic resistance, the desired gain must respect the following condition:

$$g_0 < g_{0\max} = \frac{(1-r^2)g}{2}. \quad (63)$$

#### 4) SYNTHESIS OF RESISTANCE Z

This characteristic impedance of the feedback TL parameters can be determined by inverting equation (43). Therefore, we have the relation:

$$Z = R_x\frac{2g_0(1+a^2)+g\left[4ag_0-(1-r^2)(1+a^2)\right]}{(1-a^2)\left[g(1-r^2)-2g_0\right]}. \quad (64)$$

#### 5) SYNTHESIS FORMULAS OF THE TL DELAY

The feedback TL delay can be determined by inverting equation (44). It yields the following synthesis formula:

$$\tau_0 = \frac{2agR_x+(1+a^2)R_x+(1-a^2)Z}{2agR_x\frac{(a^2-1)R_x-(1+a^2)Z}{(1+a^2)R_x+(1-a^2)Z}}\tau_a. \quad (65)$$

It can be rewritten in function of $r$ knowing:

- the gain $g$:

$$\tau_0 = \frac{(1-a^2)(1-r^2)g_0g^2}{\left[g_0(a^2g+2a+g)+ag(r^2-1)\right]}\tau_a, \quad \left[2g_0+g(r^2-1)\right] \quad (66)$$

- and the impedances $R_x$ and $Z$:

$$\tau_0 = \frac{(1-r^2)\left[(1+a^2)R_x+(1-a^2)Z\right]}{4ag_0R_x^2\left[(a^2-1)R_x-(1+a^2)Z\right]}\tau_a. \quad (67)$$

Despite the analytical formulations, one may wonder about the practical feasibility of all-pass NGD function. To answer to these curious inquiries about this innovative electronic function, application results are discussed in the next section.

## V. UDCF NGD FUNCTION VALIDATION RESULTS

In order to validate the all-pass NGD function with the UDCF topology explored previously, simulations were performed. The simulations are realized in both the frequency and time domain. They are run in the commercial tool ADS® environment of the electronic circuit designer and simulator provided by Keysight Technologies®.

### A. DESCRIPTION OF THE NGD CIRCUIT PROOF OF CONCEPT

As described in previous Section II, the proposed UDCF circuit can be designed similarly to the classical and familiar electronic RF circuits. A prototype of UDCF circuit was designed and fabricated as a POC. Fig. 2 shows the schematic of the designed NGD active circuit.

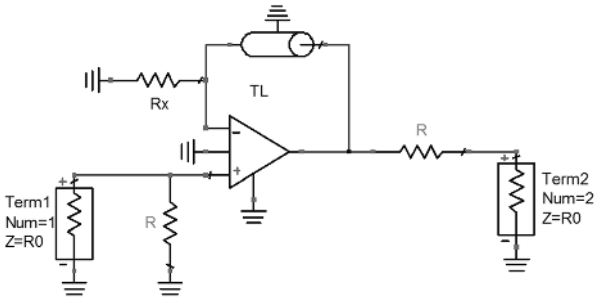


**FIGURE 2.** ADS® schematic proof of concept of the simulated UDCF NGD circuit.

This POC circuit was designed with an ideal operational amplifier presenting conversion gain $g = 20$ dB. The RF part of the circuit was designed with the input/output reflection coefficients equal to $r = -20$ dB. The feedback cable is defined by its attenuation loss $a$, physical length $d$ and dielectric effective permittivity $\varepsilon_r = 2$ which corresponds to the delay:

$$\tau_0 = \frac{d\sqrt{\varepsilon_r}}{c}, \quad (68)$$

with $c$ is the speed of light.

### B. PARAMETRIC ANALYSES WITH NUMERICAL COMPUTATION

It would be necessary to show the influences of passive and active (operational amplifier) elements onto the UDCF NGD performances before the time-domain investigation. The two following paragraphs report the obtained computational results. The parametric analyses were performed based on the S-parameter simulations from DC to 1 GHz.

#### 1) INFLUENCE OF PASSIVE ELEMENT PARAMETERS

The passive element parameters of our UDCF topology are mainly three key variables $a$, $d$ and $R_x$. Therefore, our parametric analyses in this paragraph are carried out with respect to these three characteristic variables. These passive parametric simulations were run independently. During the simulations, the concerned parameters were varied, and the other ones are fixed. Fig. 3, Fig. 4 and Fig. 5 display the simulated results of (a) GDs and (b) transmission coefficients. During the simulations, as indicated in Table 3, these three parameters were varied independently as follows:

- $a$ from 0.6 to 0.9 step 0.1,
- $R_x$ from 8 Ω to 16 Ω step 2 Ω,
- And $d$ from 0.8 m to 1.2 m step 0.1 m.

The three plotted GDs show the appearance of NGD from DC to 1 GHz. These results highlight the all pass NGD innovative function behaviors generated by the UDCF topology. Table 3 monitors the calculated GDs and transmission coefficients at very low frequencies for the considered parameters $a$, $d$ and $R_x$. As expected, the calculated results are

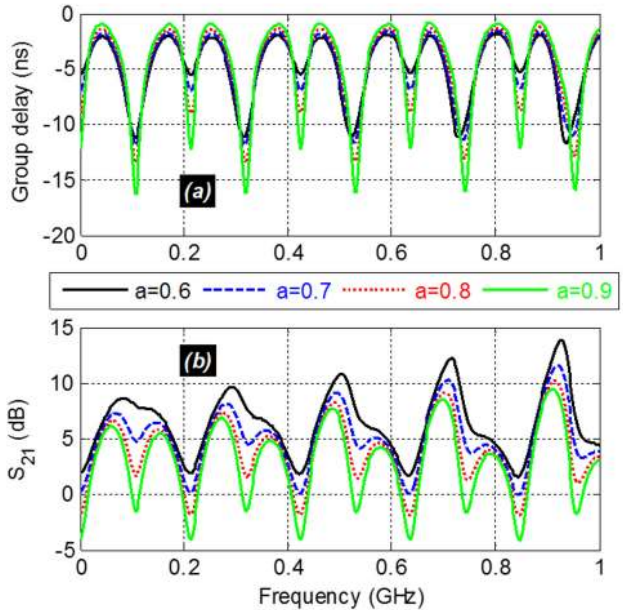


**FIGURE 3.** Simulated GD and transmission coefficient magnitude illustrating the influence of ***a***.

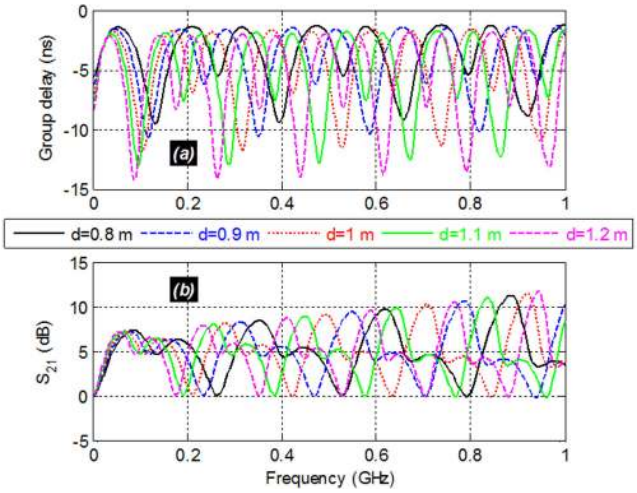


**FIGURE 4.** Simulated GD and transmission coefficient magnitude illustrating the influence of ***d***.

well-correlated to the simulations shown in Fig. 3, Fig. 4 and Fig. 5.

### 2) INFLUENCE OF THE REALISTIC OPERATIONAL AMPLIFIER BANDWIDTH

The main parameter of realistic operational amplifier susceptible to influence the all-pass NGD aspect of the UDCF topology is its bandwidth denoted $f_{OA}$ where its appropriate gain $g > 1$. In other word, if the working frequency $f > f_{OA}$, the hypothesis of equation (5) is not valid. To analyze the typically realistic influence of the operational amplifier, we varied $f_{OA}$ from 50 MHz to 0.5 GHz step 50 MHz in the present parametric simulations. After simulations of realistic operational amplifier effect, we obtain the results of GD and transmission coefficient revealed in Fig. 6(a) and Fig. 6(b), respectively. For the better interpretation, the results are

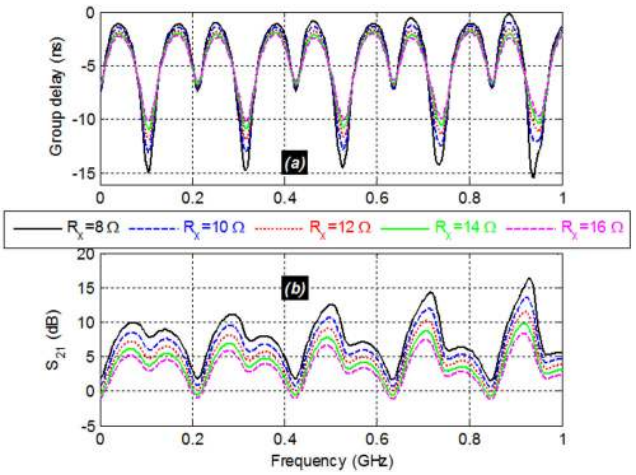


**FIGURE 5.** Simulated GD and transmission coefficient magnitude illustrating the influence of $R_x$.

**TABLE 3.** NGD levels and insertion losses at $\omega \approx 0$ from analytical prediction.

| $a$ | $d$ | $R_x$ | $\tau$ | $S_{21}$ |
|---|---|---|---|---|
| 0.6 | | | -5.4 | 1.8 dB |
| 0.7 | 1 m | | -6.9 ns | 0.1 dB |
| 0.8 | | | -9 ns | -1.8 dB |
| 0.9 | | | -12.2 ns | -3.9 dB |
| | 0.8 m | 12 Ω | -5.5 ns | |
| | 0.9 m | | -6.2 ns | |
| | 1 m | | -6.9 ns | 0.1 dB |
| | 1.1 m | | -7.6 ns | |
| | 1.2 m | | -8.3 ns | |
| 0.7 | | 8 Ω | -7.3 ns | 1.8 dB |
| | | 10 Ω | -7.1 ns | 0.9 dB |
| | 1 m | 12 Ω | -6.9 ns | 0.1 dB |
| | | 14 Ω | -6.6 | -0.4 dB |
| | | 16 Ω | -6.4 | -1 dB |

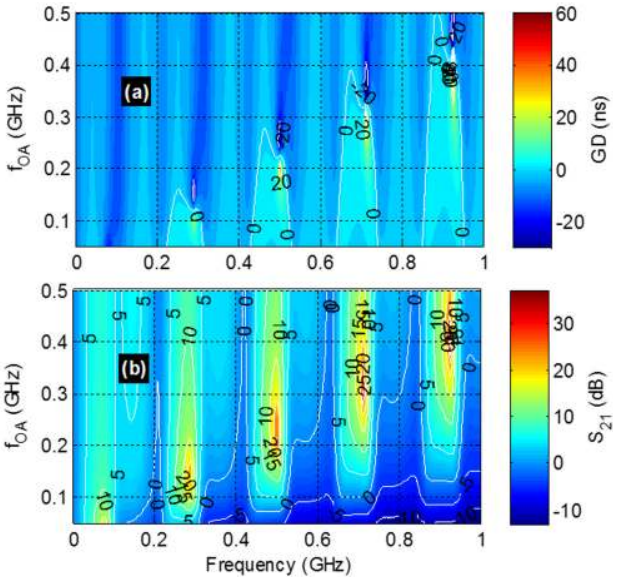


**FIGURE 6.** Cartographies of (a) GD and (b) transmission coefficient magnitude versus the working frequency $f$ and the operational amplifier bandwidth $f_{OA}$.

represented in 2-D mapped cartographies with respect to the two variables $f$ and $f_{OA}$. Two important remarks can be underlined from this active element parametric result:

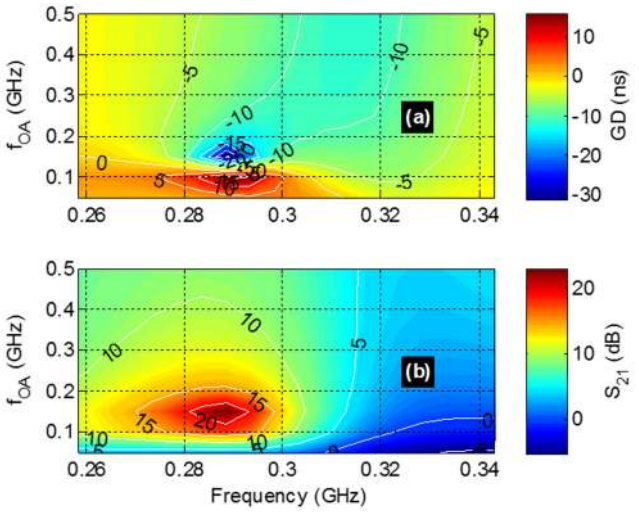


**FIGURE 7.** Zoom in of of (a) GD and (b) transmission coefficient magnitude for the working frequency band $f_{min} = 0.251$ GHz and $f_{max} = 0.341$ GHz.

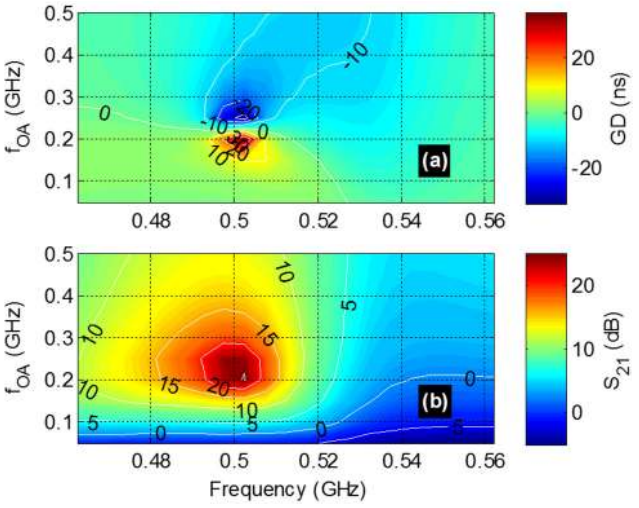


**FIGURE 8.** Zoom in of of (a) GD and (b) transmission coefficient magnitude for the working frequency band $f_{min} = 0.461$ GHz and $f_{max} = 0.561$ GHz.

- Remark 1: When considering a working frequency up to 1 GHz, the UDCF GD cannot behave as an all-pass NGD. Because as depicted in Fig. 6(a), the GD can be positive if the operational amplifier bandwidth $f_{OA}$ is sufficiently limited below 0.4 GHz.
- Remark 2: The transmission parameter can increase drastically at certain frequencies. This phenomenon can be interpreted as an instability of the UDCF topology when the operational amplifier is not perfect, or more precisely, operates with low frequency bandwidth.

For the better illustration of the operational amplifier imperfection onto the UDCF responses, four different zooms in plots of GD and $S_{21}$ are displayed in Figs. 7, Figs. 8, Figs. 9 and Figs. 10. The resonance coordinates $f$ and $f_{OA}$ of each zoomed in figure are summarized in Table 4.

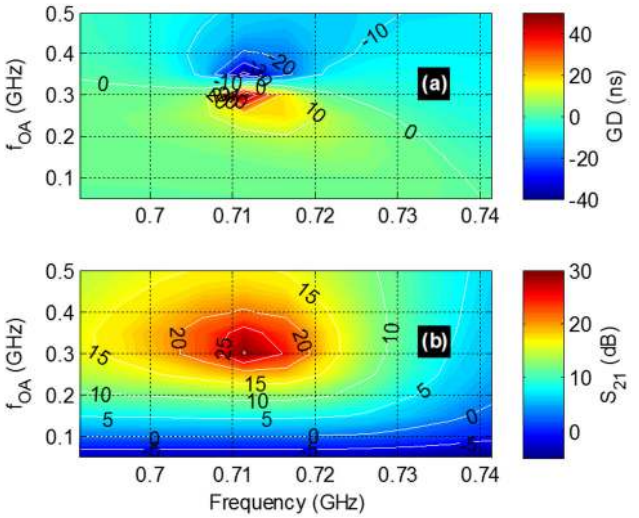


**FIGURE 9.** Zoom in of of (a) GD and (b) transmission coefficient magnitude for the working frequency band $f_{min} = 0.691$ GHz and $f_{max} = 0.741$ GHz.

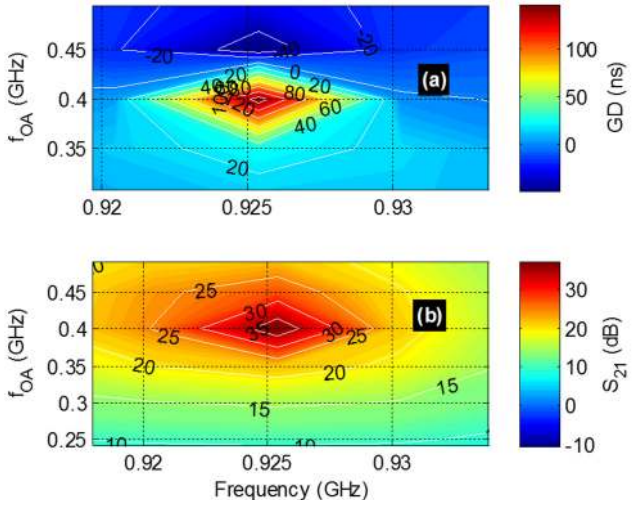


**FIGURE 10.** Zoom in of of (a) GD and (b) transmission coefficient magnitude for the working frequency band $f_{min} = 0.912$ GHz and $f_{max} = 0.938$ GHz.

**TABLE 4.** UDCF resonance coordinates for the considered range of operational bandwidth.

| *Resonance* | *1* | *2* | *3* | *4* |
|---|---|---|---|---|
| $f_{OA}$ | 0.15 GHz | 0.2 GHz | 0.3 GHz | 0.4 GHz |
| $f$ | 0.287 GHz | 0.502 GHz | 0.711 GHz | 0.925 GHz |

To get further insight about the all-pass NGD concept feasibility, more concrete simulation results by using more realistic operational amplifier and cable characteristics will be explored in the next subsection.

### C. COMPARISONS BETWEEN THE MODELLED AND SIMULATED S-PARAMETERS AND TIME-DOMAIN COMPUTATION RESULTS

The following paragraphs introduce the comparisons of the results in both frequency- and time-domain.

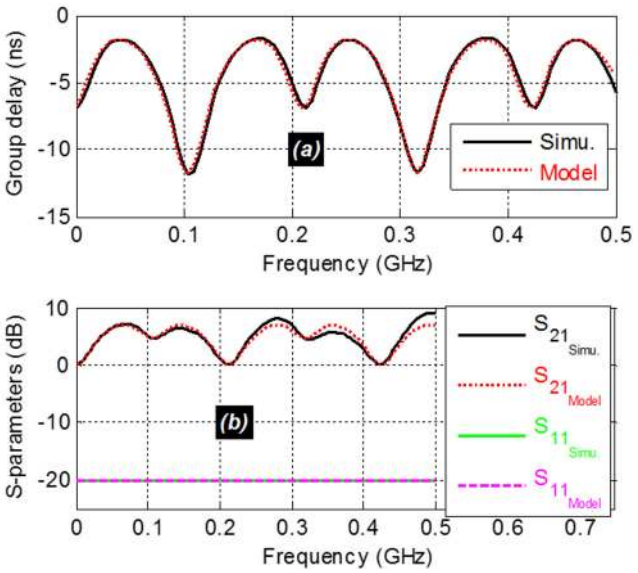


**FIGURE 11.** Comparisons of calculated and simulated (a) GD, and (b) reflection and transmission coefficient magnitudes.

### 1) DESCRIPTION OF THE UDCF POC

To perform both the frequency- and time-domain analyses, the all-pass NGD functionality of the UDCF topology was simulated with the circuit constituted by the resistance $R_x = 5\ \Omega$ and the TL cable with characteristic impedance 50 Ω and physical length $d = 1$ m. The calculations and simulations were realized with the operational amplifier model provided by the manufacturer. The simulated UDCF NGD circuit operates with an operational amplifier presenting a realistic characteristic of gain-bandwidth product.

### 2) S-PARAMETER COMPUTATIONS

The S-parameter analyses were performed from DC to 0.5 GHz. Figs. 11 display the comparisons between the modelled, and simulated GDs and the S-parameter magnitudes from the POC circuit.

A very good correlation between the analytical calculations and simulations is confirmed with these results. As expected, it can be seen in Fig. 11(a) that the all pass NGD behavior is realized up to 0.4 GHz. In the limited low frequencies, the UDCF circuit can be assumed as the NGD all-pass outstanding function. Because of the operational amplifier inherent characteristic limitation, with cut-off frequency of about 0.4 GHz of the UDCF topology under study.

At very low frequencies, the GD is approximately equal to −7 ns. As seen in Fig. 11(b), the NGD circuit demonstrator presents a very good S-parameter performance. The transmission coefficient with gain is more than 0 dB and reflection coefficient is approximately equal to −20 dB. Table 5 shows the comparative performances between the proposed UDCF and the other NGD circuits [32]–[35], [37] available in the literatures.

In the reality, the aspect of infinity NGD bandwidth depends on the operational amplifier and the used resistor components characteristics. The proposed UDCF topology enables to avoid losses and operate with very good matching under significant NGD values. Furthermore, based on the best knowledges of the authors, it is the only one NGD function presenting the all-pass NGD bandwidth.

In the considered frequency band, the calculated model and simulations of:

- GDs present an accuracy represented by the absolute differences better than 0.2 ns,
- Transmission coefficients with absolute difference lower than 2 dB,
- And Reflection coefficients with absolute difference lower than 0.1 dB.

It is noteworthy that the simulated UDCF circuit is unconditionally stable because $\mu(\omega) = 10$. Furthermore, the tested circuit presents a noise figure varying from 11 dB to 14 dB in the considered test frequency band.

### 3) TIME-DOMAIN ANALYSIS RESULTS

The better understanding about the NGD phenomenon meaning must be highlighted with time-domain analyses. In this optic, transient simulations have been conducted. The obtained results from the convolution between the S-parameters and different time-dependent test signals are discussed in this paragraph.

The three transient voltages $v_1$, $v_2$ and $v_3$ behaving as gaussian wave form with pulse width of about 80 ns and 60 ns, and arbitrary waveform are tested respectively. Figs. 12 plot the spectrums of the test signals. The test signals are typically smoothed signals presenting bandwidth belonging into the NGD bandwidth.

To perform the transient simulation, the test signal voltages are convoluted with the measured touchstone model of the POC NGD circuit prototype. Figs. 13 present the plots of the transient simulation results. It can be seen in

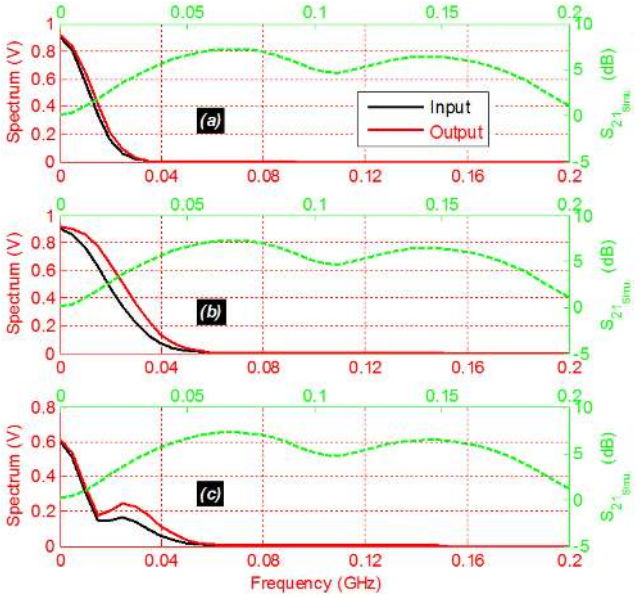


**FIGURE 12.** Spectrums of the input and output signals of (a) $v_1$, (b) $v_2$ and (c) $v_3$.

**TABLE 5. Comparison of NGD performance with the existing works.**

| *Reference* | NGD categories | NGD center frequency $f_0$ | NGD value $\tau(f_0)$ | NGD bandwidth | $S_{21}(f_0)$ | $S_{11}(f_0)$ |
|---|---|---|---|---|---|---|
| [32] | Bandpass | 1 GHz | -10 ns | 40 MHz | -20 dB | N/A (*) |
| [33] | Bandpass | 4.05 GHz | -50 ps | 3 GHz | -10 dB | N/A (*) |
| [34] | Bandpass | 50 MHz | -1 ns | 0.1 GHz | -8 dB | -3 dB |
| [35] | Low pass | DC | -5 ns | 70 MHz | -2 dB | N/A (*) |
| [37] | Bandpass | 0.5 GHz | -10 ns | 50 MHz | 0 dB | -10 dB |
| This work | All pass | Multiple with 0.1 GHz period | -12 ns | Infinity ($\infty$) | 0 dB | -20 dB |

(*) *N/A: Not applicable*

Fig. 13(a), 13(b) and 13(c) that the outputs of $v_1$, $v_2$ and $v_3$ manifest a negative time delay compared to the input.

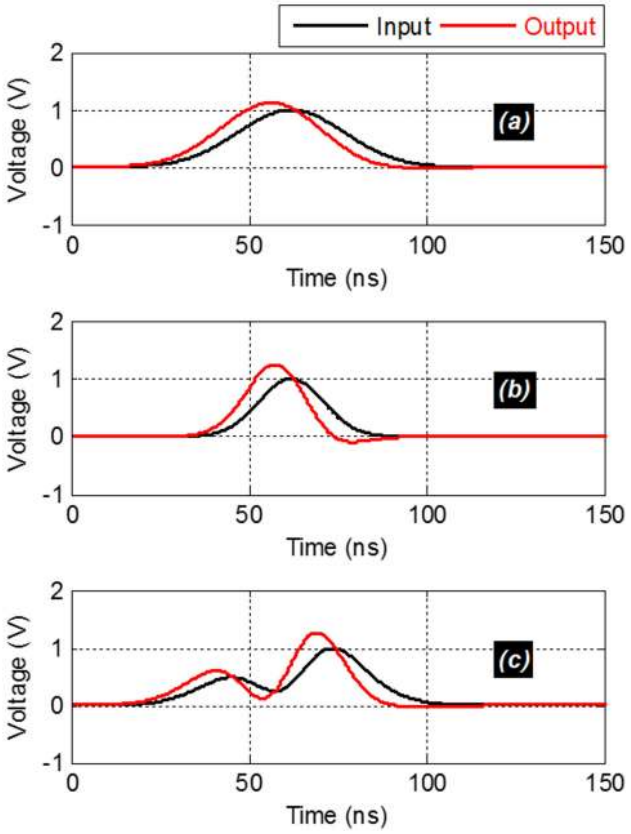


**FIGURE 13. Time-domain simulation results with input signals (a) $v_1$, (b) $v_2$ and (c) $v_3$.**

It can be emphasized that the NGD phenomenon is demonstrated by the NGD signature realistically traduced by time-advance of about −5.2 ns between the output and input signals. One more time, as pointed in [19]–[22], the NGD effect is not in contradiction with the causality.

### *D. ADVANTAGES AND DRAWBACKS OF THE PROPOSED UDCF TOPOLOGY*

Compared to the NGD circuit explored in [37], the proposed UDCF one presents certain advantages and drawbacks.

- Advantages:
  - The capacity to compensate loss with the possibility to operate with gain,
  - The possibility to operate in very wide NGD frequency band,
  - The possibility to operate in both basebands including the DC component and high frequency band,
  - The possibility to generate high NGD values at high frequencies.
- Drawbacks:
  - The design complexity with the operational amplifier,
  - The sensitivity to the operational amplifier bandwidth and gain characteristics.

## VI. CONCLUSION

A novel circuit theory of all-pass NGD function is developed. The function is elaborated with the innovative UDCF topology consisted of an operational amplifier in feedback with the network of a resistive element associated with a lossy cable. The UDCF topology theory is originally emanated with S-parameter modelling. The NGD analysis is established in function of the UDCF active cell parameters. The synthesis design method allowing to determine the circuit parameters in function of the targeted NGD specifications is proposed.

The relevance of the all-pass NGD function theory is verified with the POC design. As forecasted in theory, an outstanding original all-pass NGD function in good correlation between the theoretical model computations and simulations is obtained. Moreover, time-domain analyses illustrating the meaning of the NGD phenomenon generated by the UDCF circuit were also confirmed the feasibility of the all-pass NGD function. It was shown that the UDCF circuit enables to realize any waveform signal time advance of about minus tens nanoseconds.

Comparison of the UDCF performances compared to the existing NGD circuits [32]–[35], [37] is addressed. The main advantages and drawbacks of the UDCF topology are introduced.

## REFERENCES

[1] X. Zhao, J. Zhou, S. Zhu, C. Ma, and J.-A. Lu, "Topology identification of multiplex delayed networks," *IEEE Trans. Circuits Syst. II, Exp. Briefs*, to be published.

[2] H. Zhu, Y. Wang, and P. Li, "Distributed non-convex input-constrained consensus problem for high-order discrete-time multi-agent systems subject to switching topologies, and time delays," *IEEE Access*, vol. 7, pp. 72783–72789, May 2019.

[3] Q. Xiong, P. Lin, W. Ren, C. Yang, and W. Gui, "Containment control for discrete-time multiagent systems with communication delays and switching topologies," *IEEE Trans. Cybern.*, vol. 49, no. 10, pp. 3827–3830, Oct. 2019.
[4] X. Zhang, R. Min, D. Lyu, D. Zhang, Y. Wang, and Y. Gu, "Current tracking delay effect minimization for digital peak current mode control of DC–DC boost converter," *IEEE Trans. Power Electron.*, vol. 34, no. 12, pp. 12384–12395, Dec. 2019.
[5] Q.-K. Li and H. Lin, "Effects of mixed-modes on the stability analysis of switched time-varying delay systems," *IEEE Trans. Autom. Control*, vol. 61, no. 10, pp. 3038–3044, Oct. 2016.
[6] C.-K. Zhang, Y. He, L. Jiang, M. Wu, and H.-B. Zeng, "Delay-variation-dependent stability of delayed discrete-time systems," *IEEE Trans. Autom. Control*, vol. 61, no. 9, pp. 2663–2669, Sep. 2016.
[7] J. Shen and J. Lam, "Stability and performance analysis for positive fractional-order systems with time-varying delays," *IEEE Trans. Autom. Control*, vol. 61, no. 9, pp. 2676–2681, Sep. 2016.
[8] W. Pasillas-Lépine, A. Loría, and T.-B. Hoang, "A new prediction scheme for input delay compensation in restricted-feedback linearizable systems," *IEEE Trans. Autom. Control*, vol. 61, no. 11, pp. 3693–3699, Nov. 2016.
[9] W. Xiang, "Necessary and sufficient condition for stability of switched uncertain linear systems under dwell-time constraint," *IEEE Trans. Autom. Control*, vol. 61, no. 11, pp. 3619–3624, Sep. 2016.
[10] K. Shujaee and B. Lehman, "Vibrational feedback control of time delay systems," *IEEE Trans. Autom. Control*, vol. 42, no. 11, pp. 1529–1545, Nov. 1997.
[11] E. Fridman and U. Shaked, "An improved stabilization method for linear time-delay systems," *IEEE Trans. Autom. Control*, vol. 47, no. 11, pp. 1931–1937, Nov. 2002.
[12] L. Liu, G. Zhang, W. Li, and Z. Zuo, "Delay-dependent H-infinity control of linear descriptor systems," in *Proc. 7th World Congr. Intell. Control Automat.*, Chongqing, China, Jun. 2008, pp. 1390–1395.
[13] M. Wu, Y. He, J.-H. She, and G.-P. Liu, "Delay-dependent criteria for robust stability of time-varying delay systems," *Automatica*, vol. 40, no. 8, pp. 1435–1439, Aug. 2004.
[14] K. Gu, "An integral inequality in the stability problem of time-delay systems," in *Proc. 39th IEEE Conf. Decis. Control*, Sydney, NSW, Australia, Dec. 2000, pp. 2805–2810.
[15] E. C. Heyde, "Theoretical methodology for describing active and passive recirculating delay line systems," *Electron. Lett.*, vol. 31, no. 23, pp. 2038–2039, Nov. 1995.
[16] G. Groenewold, "Noise and group delay in active filters," *IEEE Trans. Circuits Syst. I, Reg. Papers*, vol. 54, no. 7, pp. 1471–1480, Jul. 2007.
[17] C. Wijenayake, Y. Xu, A. Madanayake, L. Belostotski, and L. T. Bruton, "RF analog beamforming fan filters using CMOS all-pass time delay approximations," *IEEE Trans. Circuits Syst. I, Reg. Papers*, vol. 59, no. 5, pp. 1061–1073, May 2012.
[18] D. Solli, R. Y. Chiao, and J. M. Hickmann, "Superluminal effects and negative group delays in electronics, and their applications," *Phys. Rev. E, Stat. Phys. Plasmas Fluids Relat. Interdiscip. Top.*, vol. 66, no. 5, pp. 056601-1–056601-5, 2002.
[19] M. W. Mitchell and R. Y. Chiao, "Negative group delay and 'fronts' in a causal system: An experiment with very low frequency bandpass amplifiers," *Phys. Lett. A*, vol. 230, nos. 3–4, pp. 133–138, Jun. 1997.
[20] M. W. Mitchell and R. Y. Chiao, "Causality and negative group delays in a simple bandpass amplifier," *Amer. J. Phys.*, vol. 66, no. 1, pp. 14–19, Nov. 1998.
[21] T. Nakanishi, K. Sugiyama, and M. Kitano, "Demonstration of negative group delays in a simple electronic circuit," *Amer. J. Phys.*, vol. 70, no. 11, pp. 1117–1121, Nov. 2002.
[22] M. Kitano, T. Nakanishi, and K. Sugiyama, "Negative group delay and superluminal propagation: An electronic circuit approach," *IEEE J. Sel. Topics Quantum Electron.*, vol. 9, no. 1, pp. 43–51, Jan./Feb. 2003.
[23] N. S. Bukhman and S. V. Bukhman, "On the negative delay time of a narrow-band signal as it passes through the resonant filter of absorption," *Radiophys. Quantum Electron.*, vol. 47, no. 1, pp. 66–76, 2004.
[24] J. N. Munday and R. H. Henderson, "Superluminal time advance of a complex audio signal," *Appl. Phys. Lett.*, vol. 85, no. 3, pp. 503–505, Jul. 2004.
[25] J. N. Munday and W. M. Robertson, "Observation of negative group delays within a coaxial photonic crystal using an impulse response method," *Opt. Commun.*, vol. 273, no. 1, pp. 32–36, May 2007.
[26] H. U. Voss, "Signal prediction by anticipatory relaxation dynamics," *Phys. Rev. E, Stat. Phys. Plasmas Fluids Relat. Interdiscip. Top.*, vol. 93, no. 5, pp. 030201-1–030201-6, 2016.
[27] H. U. Voss, "A simple predictor based on delay-induced negative group delay," pp. 1–13, 2016, *arXiv:1606.07791*. [Online]. Available: https://arxiv.org/abs/1606.07791
[28] H. U. Voss, "The leaky integrator with recurrent inhibition as a predictor," *Neural Comput.*, vol. 28, no. 8, pp. 1498–1502, Aug. 2016.
[29] H. U. Voss and N. Stepp, "A negative group delay model for feedback-delayed manual tracking performance," *J. Comput. Neurosci.*, vol. 41, no. 3, pp. 295–304, Dec. 2016.
[30] M. Kandic and G. E. Bridges, "Asymptotic limits of negative group delay in active resonator-based distributed circuits," *IEEE Trans. Circuits Syst. I, Reg. Papers*, vol. 58, no. 8, pp. 1727–1735, Aug. 2011.
[31] M. Kandic and G. E. Bridges, "Limits of negative group delay phenomenon in linear causal media," *Prog. Electromagn. Res.*, vol. 134, pp. 227–246, Nov. 2013.
[32] S. Lucyszyn, I. D. Robertson, and A. H. Aghvami, "Negative group delay synthesizer," *Electron. Lett.*, vol. 29, no. 9, pp. 798–800, Apr. 1993.
[33] C. D. Broomfield and J. K. A. Everard, "Broadband negative group delay networks for compensation of microwave oscillators and filters," *Electron. Lett.*, vol. 36, no. 23, pp. 1931–1933, Nov. 2000.
[34] B. Ravelo, "Innovative theory on multiband NGD topology based on feedback-loop power combiner," *IEEE Trans. Circuits Syst. II, Exp. Briefs*, vol. 63, no. 8, pp. 738–742, Aug. 2016.
[35] B. Ravelo, "Methodology of elementary negative group delay active topologies identification," *IET Circuits Devices Syst.*, vol. 7, no. 3, pp. 105–113, May 2013.
[36] B. Ravelo, "Similitude between the NGD function and filter gain behaviours," *Int. J. Circuit Theory Appl.*, vol. 42, no. 10, pp. 1016–1032, Oct. 2014.
[37] F. Wan, N. Li, B. Ravelo, Q. Ji, B. Li, and J. Ge, "The design method of the active negative group delay circuits based on a microwave amplifier and an RL-series network," *IEEE Access*, vol. 6, pp. 33849–33858, 2018.
[38] B. Ravelo, "Theory on negative time-delay looped system," *IET Circuits, Devices Syst.*, vol. 12, no. 2, pp. 175–181, Mar. 2018.
[39] B. Ravelo, "Unity direct chain with feedback series impedance based innovative negative group delay circuit," *Int. J. Electron. Commun.*, vol. 91, pp. 11–17, Jul. 2018.
[40] F. Wan, T. Gu, B. Ravelo, B. Li, J. Q. Cheng Yuan, and J. Ge, "Negative group delay theory of a four-port RC-network feedback operational amplifier," *IEEE Access*, vol. 7, pp. 75708–75720, Dec. 2019.
[41] P. K. Chan and M. D. F. Schlag, "Bounds on signal delay in RC mesh networks," *IEEE Trans. Comput.-Aided Design Integr. Circuits Syst.*, vol. 8, no. 6, pp. 581–589, Jun. 1989.

**BLAISE RAVELO** (M'09) is currently a University Full Professor with NUIST, Nanjing, China. He is a pioneer of the negative group delay (NGD) concept about t<0 signal travelling physical space. This extraordinary concept is potentially useful for anticipating and prediction all kind of information. He was a Research Director of nine Ph.D. students (seven defended), postdocs, research engineers, and master internships. With US, Chinese, Indian, European, and African partners, he is actively involved and contributes on several international research projects (ANR, FUI, FP7, INTERREG, H2020, Euripides$^2$, Eurostars, and so on). He is a member of research groups (IEEE, URSI, GDR Ondes, and Radio Society) and coauthors of more than 240 scientific research articles in new technologies published in international conferences and journals. He is a Lecturer of circuit and system theory, STEM (science, technology, engineering, and maths), and applied physics. His research interests include multiphysics and electronics engineering. He is regularly invited to review articles submitted for publication to international journals (the IEEE TRANSACTIONS ON MICROWAVE THEORY AND TECHNIQUES, IEEE TRANSACTIONS ON CIRCUITS AND SYSTEMS, IEEE TRANSACTIONS ON ELECTROMAGNETIC COMPATIBILITY, IEEE TRANSACTIONS ON INDUSTRIAL ELECTRONICS, IEEE ACCESS, IET CDS, IET MAP, and so on) and books (Wiley and Intech Science). He is a member of IET *Electronics Letters* editorial board as circuit and system subject Editor. He has been a member of scientific technical committee of Advanced Electromagnetic Symposium (AES), since 2013. His Google scholar H-index in 2019 is 18.

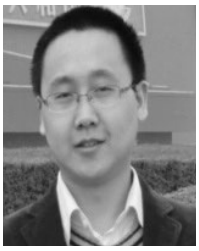

**FAYU WAN** received the Ph.D. degree in electronic engineering from the University of Rouen, Rouen, France, in 2011. From 2011 to 2013, he was a Postdoctoral Fellow with the Electromagnetic Compatibility Laboratory, Missouri University of Science and Technology, Rolla. He is currently a Full Professor with the Nanjing University of Information Science and Technology, Nanjing, China. His current research interests include negative group delay circuits, electrostatic discharge, electromagnetic compatibility, and advanced RF measurement.

**JIAO FENG** received the B.Eng. and M.Sc. degrees in communications engineering from Jilin University, Jilin, China, in 2007 and 2009, respectively, and the Ph.D. degree in wireless communications from Southampton University, U.K., in 2014. Since 2014, she has been with the School of Electric and Information Engineering, Nanjing University of Information Science and Technology, China. She is involved in the projects sponsored by the National Natural Science Foundation and by the Natural Science Foundation of Jiangsu Province. Her research interests include cooperative communication, network protocols, digital signal processing, cognitive radio networks, matching theory, machine learning, and natural language processing.